Наносистеми, наноматеріали, нанотехнології
Nanosistemi, Nanomateriali, Nanotehnologii
2020, т. 18, № 3, сс. 697–706

PACS numbers: 61.05.Lp, 68.43.Mn, 68.43.Nr, 78.40.-q, 78.67.Bf, 81.16.Hc, 82.50.Hp

Structure and Photocatalytic Properties of SnO_2 Doped with Titanium

M. Samsonenko[1], S. Khalameida[1], V. Sydorchuk[1], A. Lakhnik[2], and L. Kotynska[1]

[1]*Institute for Sorption and Problems of Endoecology, N.A.S. of Ukraine, 13, Naumov Str., UA-03164 Kyiv, Ukraine*
[2]*G. V. Kurdyumov Institute for Metal Physics, N.A.S. of Ukraine, 36, Academician Vernadsky Blvd., UA-03142 Kyiv, Ukraine*

The analysis of the changes in structural, electronic, and photocatalytic properties of tin dioxide doped with titanium oxy-hydroxide $TiO(OH)_2$ by ultrasonic treatment of wet gel is carried out. The doped samples are characterized using XRD with a full profile analysis of the diffraction patterns, N_2 adsorption–desorption and UV–Vis spectroscopy. The absence of TiO_2-phase reflections after calcining at 300–550°C and the changes in the lattice parameters *a* and *c* for the doped samples compared to the pure SnO_2 indicate the possible formation of solid solution. As a result of doping, more open meso-macroporous structure accessible for dyes molecules (Rhodamine B and Safranin T) is formed. Narrowing the band gap E_g and an increase in the absorption of visible light up to 10% at a wavelength of 550 nm are also observed. The doped sample, that is a solid solution based on SnO_2, has the highest photocatalytic activity in process of degradation of organic pollutants under visible irradiation.

Проаналізовано зміни структурних, електронних і фотокаталітичних властивостей діоксиду олова допованого оксигідроксидом титану $TiO(OH)_2$ за ультразвукового оброблення вологого ґелю. Доповані зразки були охарактеризовані за допомогою метод: РФА з повнопрофільною аналізою дифрактограм, адсорбції–десорбції N_2 й електронної спектроскопії. Відсутність піків фази TiO_2 після прожарювання при 300–550°C та зміни параметрів ґратниці *a* і *c* для допованих зразків порівняно з вихідним SnO_2 свідчать про можливе утворення твердого розчину. В результаті допування утворюється більш відкрита мезо-макропорувата структура, яка доступна для молекул барвників (Родаміну Б і Сафраніну Т). Також після допування та наступного термічного оброблення спостерігається звуження ширини забороненої зони E_g і збільшення поглинання видимого світла

до 10% за довжини хвилі у 550 нм. Допований зразок, який є твердим розчином на основі SnO_2, має найвищу фотокаталітичну активність у процесі деґрадації органічних забруднювачів за дії видимого світла.

Key words: SnO_2, titanium, ultrasonic doping, solid solution, meso-macroporous structure, visible irradiation.

Ключові слова: SnO_2, титан, ультразвукове допування, твердий розчин, мезо-макропорувата структура, видиме опромінення.

(Received 4 December, 2019)

1. INTRODUCTION

Tin dioxide SnO_2 is a wide band gap *n*-type semiconductor, which pays major attention in the fields of solar cells, gas sensors, lithium-ion batteries and photocatalysis. However, the broadband gap and slight absorption of radiation with wavelength > 400 nm prevent its photocatalytic activity under visible light. In general, the photocatalytic activity of oxides depends on multiple factors: crystal, surface and porous structure, specific surface area value, presence of structural (native) defects and impurities. A major limitation of any photocatalytic process originates from charge carrier recombination. An important approach to counteract charge carrier recombination is based on the coupling of different semiconductor components with desirable matching of their electronic band structures. As a rule, introduction of such 'extrinsic' defects into oxides structure, *i.e.*, their doping with metal or non-metal is one of the ways to improve the photocatalytic properties in processes of pollutants degradation, especially under the influence of visible light [1]. Particularly, SnO_2 and TiO_2 are central to photocatalysis [1]. As a result, of composite formation upon generation of heterointerfaces, light-induced charge separation takes place. Both oxides belong to the same crystal symmetry (tetragonal) with the space group D14 4h and two molecular units per primitive unit cell. They both crystallize within the rutile structure. Hence, they can easily form a solid solution. In addition, according to the Goldschmidt rule and Ringwood's modification [2], as a result of doping, isomorphic replacement in the crystal structure is possible: dopant ions (atoms) can replace the ions (atoms) of elements in the crystal lattice of oxide matrices. This substitution (full or partial) is possible, if several conditions are satisfied: /i/ ionic radii of metal differ by no more than 30%; /ii/ electrical neutrality of the crystal is maintained; /iii/ electronegativity of metals differs by no more than 0.4. We compared the values of ionic radii of titanium [3] and its electronegativity, which was calculated using Pauling model [4] with ones calculated for tin: 83 pm and 1.96, respectively, for tin against 75 pm and 1.54 for titanium. Besides, Ti and Sn

ions are isovalent. Therefore, they can substitute each other in the solid solution. The latter is confirmed in a number studies [5–11]. Coprecipitation, sol–gel methods are most often used for preparation of such compositions. At the same time, ultrasound (UST) based on solid dispersion processes is the effective but little explored technique for doping the oxides [12].

Thus, the aim of this work is to study the possibility of isomorphic replacement of tin with titanium in crystal structure of tin dioxide using titanium oxy-hydroxide as dopant. In addition, we evaluate of the activity of doped samples in the processes of photodegradation of organic pollutants during visible irradiation.

2. EXPERIMENTAL

Initial SnO_2 was obtained in the form of gel by precipitation using ammonia. The doping was performed by ultrasonic treatment (UST) of a wet gel mixture with titanium oxy-hydroxide $TiO(OH)_2$ as doping additive (5% w/w based on titanium dioxide) at a frequency of 22 kHz and a temperature of 90°C for 2 hours using an ultrasonic generator UZD-22/44. Doped samples were dried as well as subjected to thermal treatment (TT) in air at 300 and 550°C for 4 hours.

Diffractograms were obtained using a HZG-4 diffractometer with CoK_α radiation ($\lambda = 0.179$ nm) in the discrete mode in the angular interval of 2θ from 20° to 110° with steps of $\Delta 2\theta$ equal to 0.05°. Exposure at each point was 5 s. A full profile analysis of the diffraction patterns was performed using the MAUD program [13, 14]. The porous structure was studied using nitrogen adsorption–desorption isotherms obtained with the use of an ASAP 2405N analyser (Micromeritics Instrument Corp). The specific surface area S as well as meso- and micropore volume V_{me} and V_{mi} were calculated using BET, BJH and t-methods, respectively. The total pore volume was determined by ethanol impregnation of granules of the samples dried at 150°C. The mesopore diameter d_{me} was calculated from the curves of pore size distribution (PSD), which were plotted using the desorption branch of the isotherms.

Electron spectra of powders in the wavelength range 200–800 nm were obtained on a Shimadzu UV-2450 spectrophotometer. The value of the band gap E_g was calculated by the Planck equation:

$$E_g = 1239.5/\lambda,$$

where λ is the absorption edge, nm.

The photocatalytic activity test was performed by dyes degradation in an aqueous solution; thereto, rhodamine B (RhB) and safranin T (ST) with concentration $C_0 = 1 \cdot 10^{-5}$ mol·l^{-1} were used. The change in

their concentration in the solution was controlled spectrophotometrically using the intensity of the absorption bands 552 and 520 nm during f 30–600 min. The photocatalytic degradation was carried out in a glass reactor using a 100 W LED Cool daylight lamp (Philips), which emits exclusively in the visible region and whose spectrum has a wide band of 500–700 nm with a maximum at 565 nm. A ratio of 80 mg of photocatalyst per 80 ml of dye solution was used.

3. RESULTS AND DISCUSSION

Initial precipitated sample has composition closed to oxy-hydroxide $SnO(OH)_2$ that is confirmed by DTA–TG data [12, 15]. According to the results of XRD analysis, it has a low crystalline structure, but the doped and calcined samples have a more perfect crystal structure. In spite of the strong background in the diffraction patterns, it is possible to note the shift (and in different directions) of the maxima of the reflections from the planes (110) and (101) for as-sonicated and additionally calcined doped samples compared with initial sample (Fig. 1). Full-profile analysis of the diffraction patterns revealed following (Table 1): 1) the absence of TiO_2 phase reflections after calcining at 300–550°C; 2) the changes in the lattice parameters a and c for the

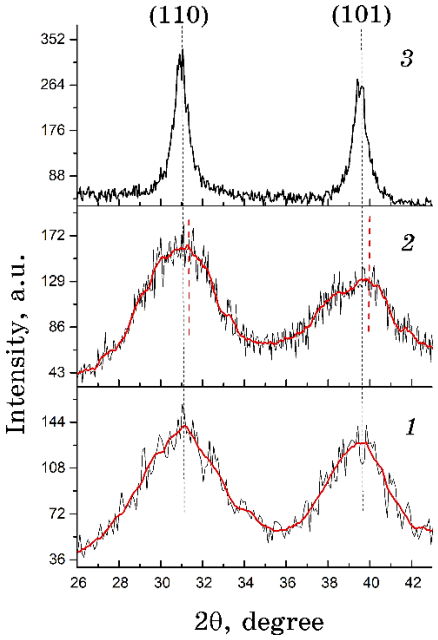

Fig. 1. XRD for SnO_2: *1*—initial, *2*—doped with titanium after UST at 90°C; *3*—doped with titanium after UST at 90°C and TT at 550°C.

TABLE 1. Unit cell parameters of initial and doped SnO_2.

No.	Sample	Lattice parameters		$\langle\varepsilon\rangle^*$	D^{**}, nm
		a b, nm	c, nm		
1	Initial SnO_2	0.4736	0.3188	0.00800	3.2
2	SnO_2 + TT 300°C	0.4744	0.3189	0.00700	5.2
3	SnO_2 + TT 550°C	0.4739	0.3188	0.00097	18.0
4	SnO_2 + 5% Ti UST 90°C	0.4748	0.3202	0.00950	3.0
5	SnO_2 + 5% Ti UST 90°C + TT 300°C	0.4740	0.3188	0.00640	4.8
6	SnO_2 +5% Ti UST 90°C + TT 550°C	0.4737	0.3185	0.00052	16.5

Note: $\langle\varepsilon\rangle^*$—the microdistortion of crystal lattice; D^{**}—the size of coherent scattering regions.

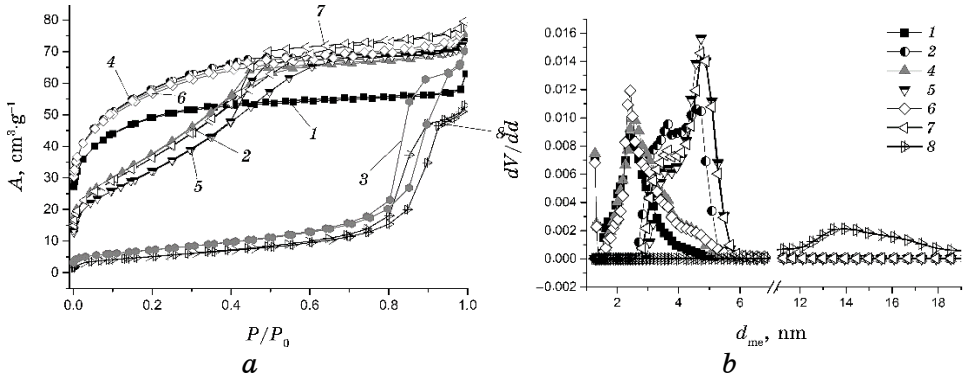

Fig. 2. Isotherms of nitrogen adsorption–desorption (*a*) and curves of PSD (*b*) for samples SnO_2 (number of the samples corresponds to the number of the samples in the Table 2.)

doped samples compared to the pure SnO_2; 3) some decrease in crystallite size D for doped samples compared with pure SnO_2 samples.

All these changes may indicate the formation of a solid solution in a doped sample. Particularly, considerable increase in a and c parameters as well as strain concentration is observed after UST of SnO_2 gel with $TiO(OH)_2$ at 95°C. Indeed, theoretical values of lattice parameters for SnO_2 (cassiterite) are following: $a = 0.47360$ nm, $c = 0.31857$ nm [16]. Calculated values for precipitated SnO_2 are 0.4736 and 0.318 nm, respectively (Table 1), which are close to theoretical values.

Significant increase in a and c parameters (0.25 and 0.44% , respectively), may indicate that titanium is embedded into the SnO_2 lattice in the

form of TiOH-species, occupying interstitial positions. Therefore, the SnO_2 cell is expanded. Next calcinations of as-sonicated doped sample is accompanied by transformation of embedded $TiO(OH)_2$ into TiO_2 with OH-groups removal [17]. Under these conditions, substitution of Sn^{4+} with Ti^{4+} in the SnO_2 lattice and formation of a solid solution becomes possible. A slight decrease in a and c parameters (by 0.04 and 0.09%, respectively) as well as increase of strain concentration for doped and calcined at 550°C sample compared with ones for pure SnO_2 calcined at 550°C (Table 1) confirm this. Taking into account that Ti^{4+} is smaller than Sn^{4+}, the SnO_2 cell is expectedly contracted.

For comparison, it can be noted that changes in a and c lattice parameters for doped with titanium SnO_2 samples were larger in [11] but titani-

TABLE 2. Porous structure parameters of the SnO_2 samples.

No.	Sample	S, $m^2 \cdot g^{-1}$	V_Σ, $cm^3 \cdot g^{-1}$	V_{ma}, $cm^3 \cdot g^{-1}$	V_{me}, $cm^3 \cdot g^{-1}$	V_{mi}, $cm^3 \cdot g^{-1}$	d_{me}, nm
1	Initial SnO_2	176	0.10	0.00	0.02	0.08	2.4
2	SnO_2 + TT 300°C	149	0.11	0.02	0.05	0.04	4.6
3	SnO_2 + TT 550°C	26	0.10	0.015	0.085	—	12.6
4	SnO_2 + UST 90°C	207	0.13	0.02	0.02	0.09	2.5
5	SnO_2 + UST 90°C + TT 300°C	125	0.14	0.03	0.07	0.04	4.7
6	SnO_2 + 5% Ti UST 90°C	201	0.21	0.095	0.03	0.085	2.4
7	SnO_2 + 5% Ti UST 90°C + TT 300°C	122	0.23	0.13	0.09	0.01	4.7
8	SnO_2 + 5% Ti UST 90°C + TT 550°C	19	0.18	0.09	0.08	0.01	13.9

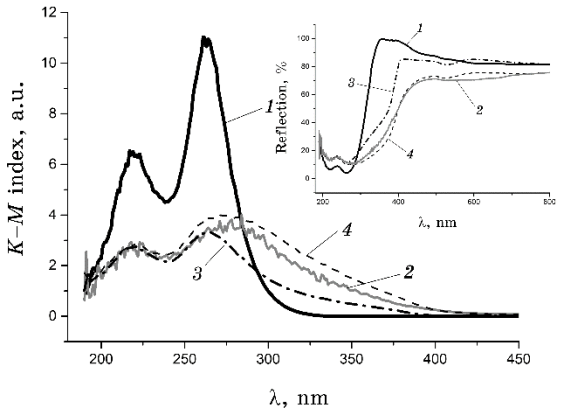

Fig. 3. Electronic spectra in the UV and visible regions for SnO_2 samples presented in co-ordinates of the Kubelka–Munk equation and the curve for reflection *vs.* wavelength (insert): *1*—initial; *2*—after TT at 300°C; *3*—doped with titanium after UST at 90°C; *4*—doped with titanium after UST at 90°C and TT at 300°C.

um contain was 10–50% in this work, and samples were calcined at higher temperature, namely 700°C.

Porous structure is also changed as a result of doping and calcinations of SnO_2 which is clearly seen from the nitrogen isotherms of adsorption–desorption: the isotherms are transformed from type I without hysteresis for initial to type IV with pronounced hysteresis for doped and calcined samples (Fig. 2, *a*). The PSD curves (Fig. 2, *b*) indicate the shift of pore size toward larger values and bi-modal structure formation as a result of doping and next calcinations.

The porous structure parameters of the doped and calcined SnO_2 samples are given in Table 2. It can be seen that UST promotes noticeable increase in specific surface area S due to some increase of micro- and mesopores content. On the contrary, following calcinations lead to significant reduction in S but increase in size of mesopores. Higher content of meso- and macropores' volume is a feature of the doped and calcined samples. Therefore, more open mesoporous or meso-macroporous structure is formed.

The bathochromic shift of the absorption edge $\Delta\lambda$ is observed on the UV–Vis spectra for doped and calcined samples (Fig. 3). As a result, the band gap E_g decreases compared to the initial sample (Table 3). Thus, the band gap E_g are 3.2 and 3.3 eV for undoped SnO_2 calcined at 300°C and 550°C, respectively. This is associated with transformation of tin oxy-hydroxide to tin dioxide [12, 18]. At the same time, E_g are 2.8, 2.9 and 2.7 eV for SnO_2 samples doped with Ti^{4+} and calcined at 300 and 550°C, respectively. Also, there is an increase in the absorption of visible light up to 10% at a wavelength of 550 nm for all the samples compared to the initial sample (inset to Fig. 3).

All samples tested shown photocatalytic activity in dyes degradation under visible illumination (Table 3, Fig. 4), which in itself is interesting. But a more important task is to compare the activity of undoped and doped samples. As can be seen from Table 3, doped samples are more active in processes RhB and ST degradation than undoped samples prepared under the same conditions (samples nos. 5 and 6 against samples nos. 2 and 3). Photocatalytic properties of semiconductors depend on their electronic characteristics, crystal and porous structure, specific surface area and degree of surface hydroxylation, and, therefore, adsorption capacity towards the substrate as well as impurities and structure defects presence [1, 10–12]. However, these factors may affect in different directions. For example, photocatalytic activity increases if specific surface area increases and band gap decreases. In this case, the specific surface area for the doped samples is lower, and the band gap for them is also smaller. As mentioned above, doped samples possess higher activity. Therefore, influence of electronic characteristics prevails. The latter are determined by presence of a solid solution (see above). Its formation is accompanied by the occurrence of dis-

TABLE 3. Photocatalytic properties of doped SnO_2.

No.	Sample	E_g, eV	RhB, $K_d \cdot 10^{-5}$, s^{-1}	ST, $K_d \cdot 10^{-5}$, s^{-1}
1	Initial SnO_2	4.2	9.2	4.5
2	SnO_2 + TT 300°C	3.2	2.2	3.6
3	SnO_2 + TT 550°C	3.3	1.6	1.0
4	SnO2 + UST 90°C	4.2	12.5	-
5	SnO_2 + 5% Ti UST 90°C	2.8	6.0	3.9
6	SnO_2 + 5% Ti UST 90°C + TT 300°C	2.9	7.7	3.2
7	SnO_2 + 5% Ti UST 90°C + TT 550°C	2.7	8.1	5.4

K_d—rate constant of Rhodamine *B* and Safranin *T* degradation.

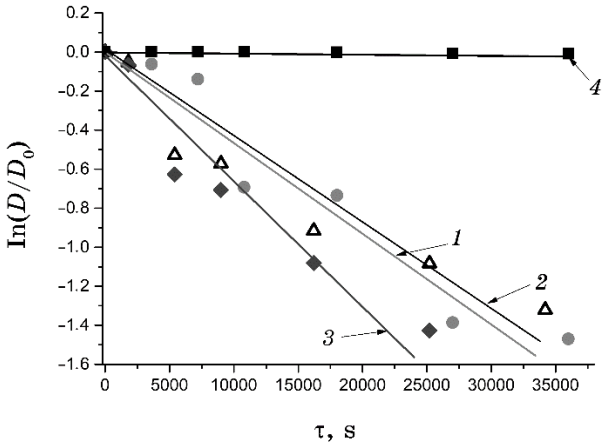

Fig. 4. Kinetic curves for the degradation of Safranin *T* in the presence of SnO_2: *1*—initial; *2*—after TT at 550°C; *3*—doped with titanium after UST at 90°C and TT at 550°C; *4*—without photocatalyst.

tortions, which manifest itself in an increase in strain concentration. These defects of structure can reduce the electron–hole recombination rate (acting like a hole capturer) and, as a result, increase the activity of the photocatalyst [10, 19].

Convincing evidence of this can be the activity of the doped sample, calcined at 550°C, in the process of Safranin degradation. Indeed, this sample showed maximal activity: rate constant of Safranin T degradation K_d is $5.4 \cdot 10^{-5}$ s^{-1} that is 1.2 times more than for pure SnO_2, although the specific surface area of the latter is 9 times higher, and the

content of surface OH-groups is 90% less. Therefore, the main reason for increased activity is precisely the presence of a solid solution in photocatalyst.

4. CONCLUSIONS

Ultrasonic doping of SnO_2 with titanium oxy-hydroxide on the stage of wet gel allows to change the structure parameters of resulted composition over a wide range. Calcined at 550°C sample, that is a solid solution based on SnO_2, has meso-macroporous structure and the highest photocatalytic activity under visible irradiation in process of dyes degradation in aqueous medium.

REFERENCES

1. M. R. Hoffmann, S. T. Martin, W. Choi, and D. W. Bahneman, *Chem. Rev.*, **95**: 69 (1995).
2. J. N. Lalena and D. A. Cleary, *Principles of Inorganic Materials Design* (New Jersey: John Wiley and Sons: 2010).
3. R. D. Shannon, *Acta Cryst. A*, **32**: 751 (1976).
4. W. B. Jensen, *J. Chem. Educ.*, **73**, No. 1: 11 (1996).
5. J. Lin, J. C. Yu, D. Lo, and S. K. Lam, *J. Catal.*, **183**: 368 (1999).
6. K. Zakrzewska and M. Radecka, *Procedia Engineering*, **47**: 1077 (2012); https://doi.org/10.1016/j.proeng.2012.09.337.
7. K. Sakthiraj, and K. B. Kumar, *Int. J. ChemTech Res.*, **6**, No. 3: 2216 (2014).
8. S. M. Hassan, A. I. Ahmed, and M. A. Mannaa, *Journal of Science: Advanced Materials and Devices*, **4**, No. 3: 400 (2019); https://doi.org/10.1016/j.jsamd.2019.06.004.
9. X. M. Liu, S. L. Wu, P. K. Chu, J. Zheng, and S. L. Li, *Materials Science and Engineering: A*, **426**, Nos. 1–2: 274 (2006); https://doi.org/10.1016/j.msea.2006.04.032.
10. L. Ran, D. Zhao, X. Gao, and L. Yin, *Cryst. Eng. Comm.*, **17**, No. 22: 4225 (2015); https://doi.org/10.1039/c5ce00184f.
11. Y. Cao, W. Yang, W. Zhang, G. Liu, and P. Yue, *New Journal of Chemistry*, **28**, No. 2: 218 (2004); https://doi.org/10.1039/b306845e.
12. S. V. Khalameida, M. N. Samsonenko, V. V. Sydorchuk, V. L. Starchevskyy, O. I. Zakutevskyy, and O. Yu. Khyzhun, *Theor. Exp. Chem.*, **53**, No. 1: 40 (2017); https://doi.org/10.1007/s11237-017-9499-5.
13. L. Lutterotti, S. Matthies, and H.-R. Wenk, *Proc. of the 12th International Conf. on Textures of Materials (ICOTOM-12) (August 9–13, 1999)* (Ottawa: NRC Research Press: 1999), vol. **1**, p. 1599.
14. L. Lutterotti, S. Matthies, and H.-R. Wenk, *IUCr: Newsletter of the CPD*, **21**: 14 (1999).
15. M. Samsonenko, O. Zakutevskyy, S. Khalameida, B. Charmas, and J. Skubiszewska-Zięba, *Adsorption*, **25**, No. 3: 451 (2019); https://doi.org/10.1007/s10450-019-00036-2.
16. *Landolt-Börnstein. Numerical Data and Functional Relationships in Science*

and Technology (Ed. O. Madelung) (Berlin: Springer: 1983), vol. **17**, p. 133.
17. M. Irani, K. A. M. Gasem, B. Dutcher, and M. Fan, *Fuel*, **183**: 601 (2016); https://doi.org/10.1016/j.fuel.2016.06.129.
18. S. Khalameida, M. Samsonenko, J. Skubiszewska-Zięba, and O. Zakutevskyy, *Adsorption Science and Technology*, **35**, Nos. 9–10: 853 (2017); https://doi.org/10.1177/0263617417722251.
19. M. Crişan, D. Mardare, A. Ianculescu, N. Drăgan, I. Niţoi, D. Crişan, and B. Vasile, *Applied Surface Science*, **455**: 201 (2018); https://doi.org/10.1016/j.apsusc.2018.05.124.